PHYSICAL REVIEW A VOLUME 21, NUMBER 5 MAY 1980

Experimental limits on deviations from Z^2 dependence of Čerenkov radiation by heavy ions

M. H. Salamon, S. P. Ahlen, and G. Tarlé
Department of Physics and Space Sciences Laboratory, University of California, Berkeley, California 94720
(Received 12 October 1979)

We have exposed a variety of Čerenkov radiators to relativistic Ne, Ar, and Fe ions at the Lawrence Berkeley Laboratory's Bevalac and have examined the charge dependence of the Čerenkov emission. Classically, and to first order in relativistic quantum theory, the dependence is Z^2, although certain higher-order corrections suggest a Z^4 dependence as well. Our experimental results are consistent with a pure Z^2 dependence and limits are placed on Z^3 and Z^4 higher-order contributions to Čerenkov emission, whose theoretical bases are briefly discussed. In addition to primary Čerenkov emission, we discuss light sources such as Čerenkov emission by secondary electrons, saturated radiator scintillation, and others which are confronted in most experimental configurations incorporating Čerenkov radiators.

I. INTRODUCTION

The agreement between experiment and the theoretical expression for Čerenkov radiation intensity[1,2] has been well established for singly charged particles.[3] For relativistic particles of higher charge Ze the classical Čerenkov formula predicts that the intensity scales simply as Z^2e^2 for a given particle velocity. Although widely accepted, this has never been experimentally verified for $Z>1$ due to the previous unavailability of relativistic, highly charged particles of accurately known energies. Verification or refutation of this scaling would have both experimental and theoretical significance: First-order calculations in the quantum electrodynamics of material media directly produce the classical Čerenkov formula,[4-6] but higher-order calculations for relativistic electrons contribute terms proportional to e^4 as well,[7,8] suggesting the existence of similar Z^4e^4 corrections for heavy ions. This, or other deviations from Z^2 dependence, could lead to serious difficulties in present cosmic-ray experiments measuring high Z elemental abundances which incorporate Čerenkov radiators as part of a charge identification scheme.[9]

Motivated by these considerations, we exposed wave-shifted and non-wave-shifted Čerenkov radiator samples to relativistic Ne, Ar, and Fe ions at Lawrence Berkeley Laboratory's heavy-ion accelerator, the Bevalac (capable at present of accelerating ions of up to $Z=26$ to energies up to 2 GeV/amu), during runs primarily devoted to examining scintillation response of various media to heavy ions. The experimental configuration and calibration techniques are discussed in the next section. Analysis of the data, the content of Sec. III, revealed several contributions to the recorded response curves which must be considered in many detector configurations in order to achieve high primary Čerenkov signal accuracy. These include delta-ray (secondary electron) Čerenkov emission, background air scintillation, Čerenkov radiator scintillation (discussed in Sec. V), light escape efficiency corrections (geometrical in origin, and dependent upon particle velocity), as well as others more peculiar to the particular experimental configuration. The result of the analysis is that no significant deviation from Z^2 dependence is observed, placing limits on the magnitude of any higher-order terms in Z that might be theoretically expected in the Čerenkov formula. These conclusions are discussed in Sec. VI. Section IV deals briefly with the theoretical issue of terms of higher order in Z in the Čerenkov formula.

II. EXPERIMENTAL CONFIGURATION

Four 1.27-cm-thick Čerenkov radiator samples were tested: a pair of samples of ultraviolet-transmitting acrylic (UVTA), a common radiator material, and a pair of samples of Pilot 425,[10] which is acrylic doped with a wave shifter (WSA). The wave shifter absorbs uv light and reradiates in the visible to allow transmission through non-quartz photomultiplier tube windows. One sample of each pair was roughened (R) on all sides by sandblasting, a common technique intended to eliminate signal dependence on incident particle trajectory, while the other was kept smooth (S). In addition to testing for deviations from a Z^2 dependence, this selection allowed a comparison of relative light outputs (radiator efficiencies) and radiator scintillation-to-Čerenkov ratios, since the scintillation component is a background contaminant that, unlike all other background light sources, does not scale as Z^2 due to ionization quenching.[11] (See Sec. V.) Testing smooth (S) versus roughened (R) radiator samples mea-

sured the effectiveness of roughening in removing surface geometrical signal distortions. The four samples were exposed to the Fe beam, but time limitations during the Ar and Ne exposures allowed only the UVTA, R and WSA, R samples to be exposed to Ne and only the WSA, R sample to be exposed to Ar.

The 600-MeV/amu fixed-energy beams of Ne, Ar, and Fe were incident on a discretely variable, extremely high precision lead absorber, shown in Fig. 1, enabling rapid, accurate variation of the beam energy at the radiator. A solid-state detector (SSD) discriminated against those ions that had undergone charge-changing nuclear interactions within the absorber. The ions then passed through an opaque window, a very thin air gap, the (nonoptically coupled) Čerenkov radiator, and then exited through the interior of a light diffusion box containing 20 in. of air.[12] The opaque window is a 1.27-cm-thick piece of polyvinyltoluene (PVT), dyed with Sudan Black to minimize its own Čerenkov and scintillation emission; it is present to compensate for loss of delta rays (which contribute appreciably to the light output) out the radiator interior face by providing a comparable spectrum of delta rays at the radiator exterior face. The radiator and window thicknesses were chosen to match the range[13,14] of the maximum-energy delta rays produced by 600-MeV/amu ions to ensure proper delta-ray compensation.

The light emitted by the radiator was radiated into the interior of a light diffusion box coated with a highly reflectant layer[15,16] of $BaSO_4$ (having nearly wavelength-independent reflection coefficient) which randomized the light before it reached the photomultiplier tube (PMT). Computer calculations[17] indicate negligible response variation with shift in particle entry position on the sample surface. The light was detected by an EMI9817-QAM quartz-window PMT. This tube was tested for possible nonlinearity by measuring the Poisson-distributed output of a light-emitting

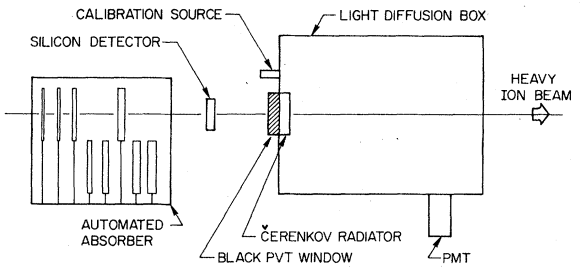

FIG. 1. Experimental configuration. The exterior face of the radiator is that which faces the black PVT window.

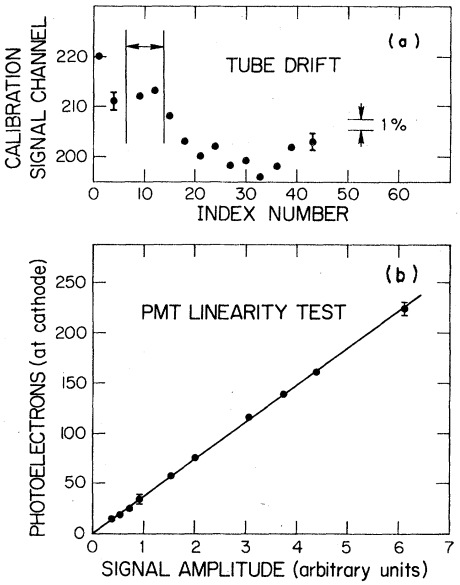

FIG. 2. (a) Intrarun calibration data (for WSA, R:Ne). The nth measurement in a run is assigned index number n. The bars piercing the data mark the cluster of measurements containing a primary Čerenkov component. (b) PMT response curve. No saturation effects occur within the PMT dynode structure, since photocathode electron number scales linearly with final signal amplitude. Since the photocathode is of the low-resistance trialkali type, photoelectron number also scales linearly with photon number of given wavelength.

diode excited by a precision pulser. Full-width half-maximum measurements as a function of pulse-height-analyzer channel, after noise subtraction, provided an accurate measure of cathode photoelectron number versus final signal channel. Figure 2(b) demonstrates the linearity of the response. Temporal tube drift was corrected for by affixing an ^{241}Am-doped NaI(Tl) scintillator[18] to the light box as a constant calibration light source. Periodic calibrations were performed; Fig. 2(a) shows a particularly erratic calibration curve for one sample run. Sample light levels were calculated by linear interpolation between calibration measurements; all light outputs have been converted to units of this source (roughly equal to 400 cathode photoelectrons). Temperature variations were controlled so that the maximum possible NaI response shift over the three ions runs was $< 0.4\%$; thus, data from the three runs (spaced 48 h apart) could be compared accurately.

Inter-run comparisons using the extensive quantity of scintillation data also taken during these runs (to be published at a later date) showed a typical peak measurement accuracy of $\sim 0.5\%$ due to the statistics accompanying $\sim 10^4$–10^5 ions per analyzer spectrum.

III. ANALYSIS OF DATA

A. Spectrum components

Figure 3 shows a typical raw radiator sample response curve of light output versus beam energy at the radiator exterior face, along with the data in various phases of subtraction. The shape of the spectrum can be understood by examining its components.

1. Primary Čerenkov radiation

This is the Čerenkov radiation directly produced by the ion, and is expressible by[19] (in photoelectrons/cm)

$$\frac{dL_1}{dx}(\beta)=\frac{Z^2e^2}{\hbar c^2}F\int_{n(\omega)>1/\beta}^{\omega_c} g(\omega,\beta)q(\omega)\times\left(1-\frac{1}{n^2(\omega)\beta^2}\right)d\omega\,, \quad (1)$$

where F is the PMT collection efficiency of the detector configuration, βc is the ion velocity, $q(\omega)$ is the PMT quantum efficiency, and $n(\omega)$ is the refractive index. The probability of photon escape from the radiator, $g(\omega,\beta)$, is assumed to be factorable as $g_1(\beta)g_3(\omega)$; $g_3(\omega)$ depends upon the optical (absorptive) properties of the medium, while $g_1(\beta)$ is a β-dependent geometrical correction factor arising from the dependence of the radiator-air transmission coefficient on radiation incidence angle, itself a function of β. If we assume for UVTA that $g_3(\omega)$ is flat up to a critical self-absorption frequency ω_c, where $g_3(\omega>\omega_c)=0$, then we may approximate

$$\frac{dL_1}{dx}(\beta)=Z^2\kappa g_1(\beta)\int_{n(\omega)>1/\beta}^{\omega_c} q(\omega)\left(1-\frac{1}{n^2(\omega)\beta^2}\right)d\omega\,, \quad (2)$$

where κ is the "radiator efficiency." The commercially determined $q(\omega)$ for the PMT used is shown in Fig. 4, along with $n(\omega)$, which is determined by the single oscillator model $n^2(\omega)=1+A/(\omega_0^2-\omega^2)$, with the two parameters determined by the values $n(589\text{ nm})=1.490$, $n(425\text{ nm})=1.502$.[20] The low-frequency cutoff in $q(\omega)$ allows us to ignore the lower integral limit for $E>325$ MeV/amu. Then

$$\frac{dL_1}{dx}=Z^2\kappa g_1(\beta)\left(1-\frac{1}{n_0^2\beta^2}\right);\qquad \frac{1}{n_0^2}\equiv\int_0^{\omega_c}\frac{q(\omega)}{n^2(\omega)}d\omega\Big/\int_0^{\omega_c}q(\omega)d\omega\,, \quad (3)$$

where the radiator efficiency κ now absorbs a constant. For the observed UVTA cutoff wavelength $\lambda_c=260$ nm,[20] $n_0=1.518$. As will be seen, this is exactly the measured value of n_0, the effective refractive index, for UVTA. The effective refractive index is clearly a function of the particular PMT quantum efficiency curve.

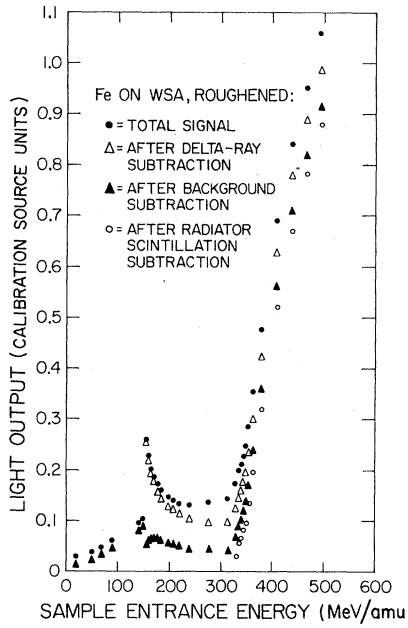

FIG. 3. Radiator response data, showing a typical sample data set in various stages of subtraction. The sample entrance energy is the ion energy at the exterior face of the radiator. The light levels are in units of the light output by the calibration source. Note the presence of delta-ray Čerenkov light well below the primary Čerenkov threshold, seen by comparing the total signal with post-delta-ray subtraction curves (see also Fig. 5). The abrupt discontinuity of the total signal at ~150 MeV/amu is due to the sudden cessation of air scintillation, as the ion energy is reduced so that it stops within the radiator. Light outputs below this energy are due to radiator scintillation plus a small background from the black PVT window. The final, pure primary Čerenkov signal (open circles) seems to deviate from its expected form near the threshold energy. This is due to the ion's energy going below threshold within the finite thickness of the radiator.

For $E<325$ MeV/amu, n_0 will depend upon β; thus, we discard primary Čerenkov data points where the ion energy is less than this over a significant fraction of the radiator thickness Δx.

The total primary Čerenkov light output $\Delta L=\int_0^{\Delta x} dL_1/dx\,dx$. We use an approximation of Cantin *et al.*[21] whereby

$$\Delta L=\int_0^{\Delta x}\frac{dL_1}{dx}dx\approx\frac{Z^2\kappa g_1(\bar\beta)}{n_0^2}\left(n_0^2-1-\frac{1}{p_i p_0}\right)\Delta x\,, \quad (4)$$

where $g_1(\bar\beta)$ is a thickness averaged $g_1(\beta)$, and $p_i=\beta_i(1-\beta_i^2)^{-1/2}$ is the ion "momentum" at the radiator external face, with p_0 being the ion "momentum" at the interior face. This approximation is surprisingly accurate in certain regimes; compu-

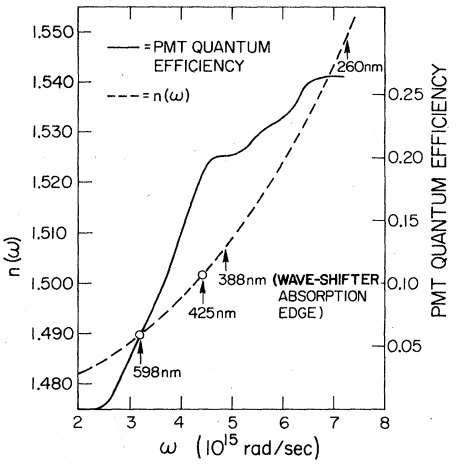

FIG. 4. PMT quantum efficiency and radiator refractive index as function of frequency. The two established refractive index values determining the $n(\omega)$ curve are shown.

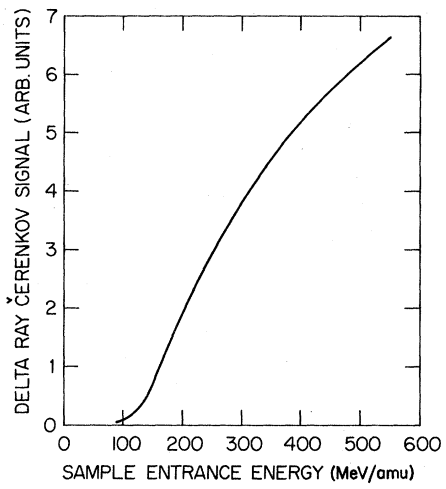

FIG. 5. Delta-ray (secondary-electron) Čerenkov emission contributing to the total signal. The specific shape of the curve depends upon the thickness of radiator and the presence or absence of adjacent upstream matter. The projectile ions threshold for delta-ray Čerenkov output is 74 MeV/amu.

ter calculations comparing the integral to the approximation show agreement to far better than 1%.

The ion energies within the radiator are calculated with range-energy programs[22] that incorporate higher-order Z corrections to stopping power[23] dE/dx to ensure higher range-energy accuracy.[24,25]

2. *Delta-ray (secondary electron) Čerenkov radiation*

The energy spectrum of delta rays produced by the primary ion is given by

$$\frac{dn}{d\epsilon dx}=\frac{2\pi NZ^2e^4}{mc^2\beta^2\epsilon^2}\left(1-\beta^2\frac{\epsilon}{\epsilon_m}\right)(\mathrm{MeV^{-1}\,cm^{-1}})$$

$$=(0.1535)\frac{Z_2}{A_2}\frac{Z^2}{\beta^2\epsilon^2}\left(1-\beta^2\frac{\epsilon}{\epsilon_m}\right)$$

$$\times(\mathrm{MeV^{-1}\,g^{-1}\,cm^2}), \qquad (5)$$

where N is the electron density of the medium, m is the electron mass, ϵ is the delta-ray energy, $\epsilon_m=2m\gamma^2\beta^2c^2$, and Z_2/A_2 is the medium-averaged atomic number to atomic weight ratio. The Čerenkov emission from each delta ray above threshold energy ϵ_0 is given by

$$\frac{dL_2}{dr}=\kappa g_2(\beta,\beta_e)\left(1-\frac{1}{n_0^2\beta_e^2}\right),$$

where $r(\epsilon)$ is the delta-ray range, $c\beta_e$ is the delta-ray velocity, and $g_1(\beta)\neq g_2(\beta,\beta_e)$, since the ion and delta-ray trajectories differ. The total delta-ray Čerenkov component is

$$\Delta L_2(\beta)=\int_0^{\Delta x}dx\int_{\epsilon_0}^{\epsilon_m}d\epsilon\,\frac{dn}{d\epsilon\,dx}\int_{r(\epsilon_0)}^{r(\epsilon)}dr\frac{dL_2}{dr}. \qquad (6)$$

Assuming $g_2(\beta,\beta_e)=1$ (i.e., neglecting temporarily for lack of knowledge any possible geometrical signal distortions), these ΔL_2 values were calculated using the scheme of Lezniak[26] to account for delta-ray loss out of the radiator and supply from the PVT window. The only modification to this scheme was the use of more accurate electron range-energy relations: the continuous slowing down approximation (CSDA) ranges of Berger and Seltzer[19] are used to calculate delta-ray Čerenkov emission, while the penetration depth relations of Kobetich and Katz[20] are used to calculate delta-ray transport. The resulting response curve is shown in Fig. 5; note the presence of delta-ray Čerenkov radiation well below the cutoff for primary Čerenkov radiation. Although the assumption $g_2(\beta,\beta_e)=1$ is necessary for a first subtraction of the delta-ray component from the raw sample response curve, we find that after integration over $d\epsilon$, the proper correction factor is quite insensitive to the ion's β; this is due to the large, fairly β-insensitive, angular distribution of delta-ray Čerenkov light (Fig. 6) that "smears" geometrical distortions. Thus, after properly accounting for geometrical effects, the delta-ray component will simply have a "radiator efficiency" $\kappa_2=\Gamma\kappa$ where $\Gamma<1$ and must be determined for each radiator type.

3. *Background*

The background consists of all contributions to the light output apart from the radiator. They include scintillation of the air within the light diffusion box, Čerenkov radiation in the $BaSO_4$

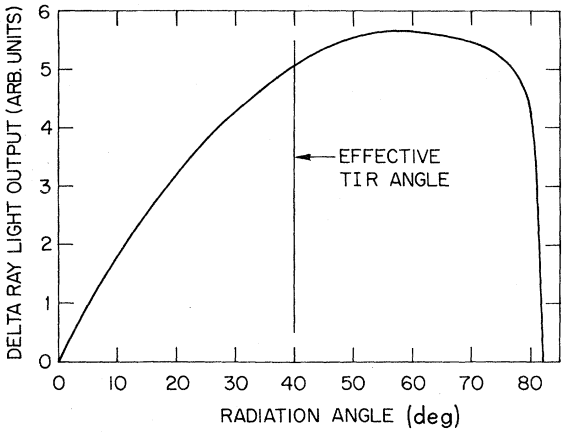

FIG. 6. Delta-ray Čerenkov light output as a function of angle relative to ion trajectory. The separate angular distributions of delta-ray production and individual delta-ray Čerenkov emission are combined to produce this remarkably β-insensitive curve. Noting the position of the effective total internal reflection (TIR) angle for smooth surfaces allows an estimate of the radiator efficiency factor Γ.

coating,[27] and very small amounts of scintillation and Čerenkov radiation from the black dyed PVT. Background (no sample) response curves were measured during the Fe (Fig. 7) and Ar runs; these were directly subtracted from the radiator sample response curves (after appropriate energy abscissa shifts) as shown in Fig. 3. For Ne, however, the background had to be reconstructed using the Fe and Ar data to calculate air scintillation efficiency, $BaSO_4$ Čerenkov emission parameters, and emission efficiency from the black PVT window; thus, the errors associated with Ne are slightly larger than for Fe or Ar.

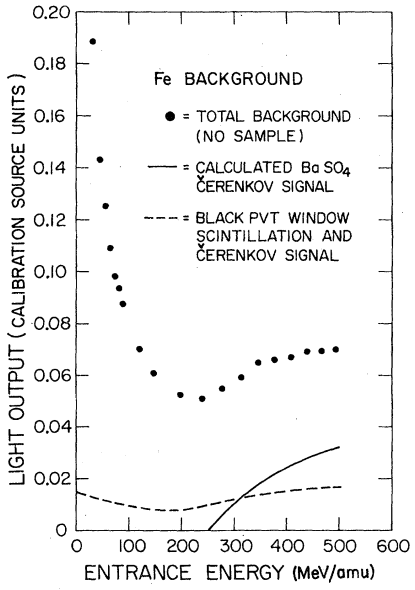

FIG. 7. Background light sources (no radiator in place). The dominant contributor is air scintillation, which monotonically decreases with sample entrance energy.

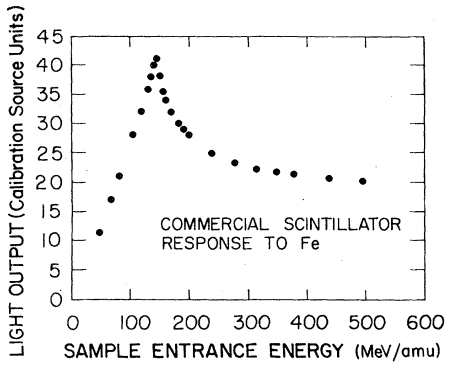

FIG. 8. Scintillation response data of a commercial scintillator (Pilot *Y*). This figure emphasizes the structure expected in the radiator scintillation component of Fig. 3 (after background subtraction). In this figure, all background light sources are negligible.

4. *Radiator scintillation*

The curve in Fig. 3 remaining after background subtraction is solely radiator light output. The peak at 150 MeV/amu corresponds to the ion stopping at the interior edge of the radiator providing maximum energy deposition and scintillation (see also Fig. 8). The discontinuity past this cusp is due to the extreme sensitivity of air scintillation subtraction to errors in calculated energy just near the particle's end of range in the air column, and is of no consequence. The "plateau" value near 300 MeV/amu is used as an estimate of the radiator scintillation component in the energy range 300–600 MeV/amu, and is treated as a constant. Comparison with a commercial scintillator spectrum (Fig. 8) shows this to be an excellent approximation.

B. Radiator parameters

1. *Geometrical corrections*

The remaining light levels ΔL follow Eq. (4). These are plotted with respect to $(1/p_i p_0)$ (which decreases for increasing energy E) for the UVTA, S:Fe and UVTA, R:Fe ΔL data in Fig. 9, where the data errors are comparable to the dot sizes. It is seen that the smooth, non-wave-shifted Čerenkov radiator has $g_1(\bar{\beta}) = 1$ (to within an indeterminable constant) for $E < 500$ MeV/amu, while the roughened, non-wave-shifted radiator has significant geometrical deviations from linearity at higher energies, as well as an overall attenua-

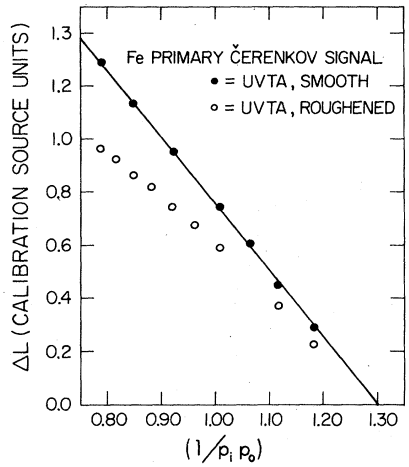

FIG. 9. Primary Čerenkov light outputs vs $(1/p_i p_0)$ for both smooth and roughened UVTA samples exposed to Fe. These two data sets are used to generate a $(1/p_i p_0)$-dependent, Z-independent ratio that will "boost," or "correct," other roughened UVTA data to linear forms.

tion relative to the smooth sample. The origin of the deviations from linearity in the ΔL vs $(1/p_i p_0)$ curves is in the variation of light transmission probability across the radiator-air surface as a function of light incidence angle at the surface. The Čerenkov light is emitted in a cone at angle $\phi = \cos^{-1}(1/n_0\beta)$ relative to the ion trajectory. A smooth surface ensures that the incidence angle $\theta \leq 30°$ for normally incident ions of $E \leq 500$ MeV/amu; over this angular range the transmission coefficient is nearly constant (Fig. 10). A roughened surface, however, presents a surface angular distribution to the oncoming Čerenkov light. Light emitted at an angle $\theta < \theta_c$, where θ_c is the total internal reflection angle, may still be totally internally reflected since the surface incidence angle is the sum of the Čerenkov emission angle and the local, finite angle of the roughened surface. Based on optical microscope measurements of the roughened surface, parameters were input to a Monte Carlo photon escape efficiency algorithm that assumed sinusoidal surface variations. The efficiency curve generated (Fig. 10) shows a decrease in transmission beginning at lower energies in roughened surfaces than in smooth ones. This curve, applied to roughened sample data, produces very good fits to straight lines, confirming the nature of the deviations, although it does not correct for attenuation.

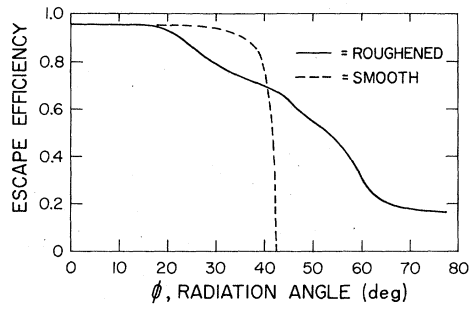

FIG. 10. Photon escape efficiency vs emission angle relative to ion trajectory for both smooth and roughened radiators.

When $g_1(\bar{\beta}) = 1$ (as it is for smooth samples), a simple linear regression analysis may be performed on the data conforming to Eq. (4) to extract values for n_0 and κ. To apply this analysis to roughened samples, however, their response curves ΔL vs $(1/p_i p_0)$ must be "corrected" by multiplying each data point by an appropriate ratio, $g_1(\bar{\beta})_{\text{smooth}}/g_1(\bar{\beta})_{\text{roughened}}$, to produce a straight line characteristic of smooth samples. This procedure is necessary because most of the data taken were with roughened radiators. These ratio curves are experimentally determined by using the Fe data of the UVTA, S, UVTA, R, and WSA, S, WSA, R samples. The wave-shifted and non-wave-shifted samples have separate correction curves $g_1(\beta)$ because wave-shifted light is isotropically reradiated, resulting in a WSA light angular distribution different from that of UVTA.

2. *Calculation of efficiencies and refractive indices*

Linear regression analysis of the UVTA, S:Fe and WSA, S:Fe data (which require no geometrical corrections) yield effective refractive indices of 1.518 (in agreement with calculation) and 1.512, respectively. The reduced n_0 for the wave-shifted sample is due to the reduced escape efficiency of the isotropically reradiated wave-shifted light, since Čerenkov light output decreases as n_0 decreases [see Eq. (4)]. The measured value of n_0 is used to calculate the escape efficiency reduction factor ρ_s for isotropic radiation within a smooth radiator. Assuming that all light of wavelength $\lambda < \lambda_a = 388$ nm (the wave shifter's effective absorption edge[28]) is wave shifted, $n_0(\rho_s)$ is calculated using Eq. (3) with the curves of Fig. 4 weighted by ρ_s in the $\lambda < \lambda_a$ region, resulting in $\rho_s = 0.55$ for $n_0 = 1.512$. This value is consistent with the expected loss of half the wave-shifted light to the black PVT window. Examination of Table I (see Sec. V), however, modifies this picture for roughened samples. The escape efficiency of isotropic light is ~1.6 times greater for roughened than for smooth surfaces, as seen by the relative magnitudes of the radiator scintillation peaks, implying $\rho_r = 0.88$. This states

TABLE I. Radiator scintillation levels (remaining after delta-ray Čerenkov and background subtractions). All light levels are in units of the calibration source. Energy deposited in the radiator for each scintillation level is shown.

	Peak	Peak ΔE (10^3MeV)	Plateau	Plateau ΔE (10^3MeV) (approx.)	$\beta = 1$ primary Čerenkov signal
WSA, R: Fe	0.085±0.005	8.44	0.045±0.010	3.6	
WSA, R: Ar	0.058±0.003	4.81	0.024±0.006	1.7	
WSA, R: Ne			0.012±0.004	0.49	
WSA, S: Fe	0.052±0.005	8.44	0.013±0.010	3.6	2.33
UVTA, R: Fe	0.025±0.005	8.44	−0.005±0.010	3.6	
UVTA, R: Ne			0.002±0.004	0.49	
UVTA, S: Fe	0.012±0.005	8.44	−0.010±0.010	3.6	3.28

that reabsorption of light reflected off the black PVT window is much more likely for roughened than for smooth surfaces.

At this point the measured relative Čerenkov light outputs of the various radiator types can actually be calculated with knowledge of the above parameters, reinforcing confidence in the model and consistency of the data. Using the expression

$$\Delta L \propto g_1(\bar{\beta})\int_0^{\omega_a} q(\omega)\left(1-\frac{1}{n^2(\omega)\bar{\beta}^2}\right)d\omega + \rho\int_{\omega_0}^{\omega_c} q(\omega)\left(1-\frac{1}{n^2(\omega)\bar{\beta}^2}\right)d\omega \qquad (7)$$

for $\bar{\beta}=0.75$, and $g_1(\bar{\beta})$ being the non-wave-shifted geometrical correction factor, one finds ΔL(WSA, R:Fe)/ΔL(UVTA, S:Fe)=0.71, compared to a measured ratio 0.68 (agreement to 4%); calculation of ΔL(WSA, S:Fe)/ΔL(UVTA, S:Fe) gives 0.62 compared to a measured ratio 0.70 (agreement to 11%). Thus, one may calculate the wave-shifted samples response given the non-wave-shifted samples response plus the ρ parameters, determined independently from refractive index and radiator scintillation measurements. [Or, equivalently, the product $\kappa g_1(\bar{\beta})$ of radiator efficiency times correction factor for WSA samples may be calculated from the $\kappa g_1(\bar{\beta})$ of the UVTA samples, allowing one to define a universal radiator efficiency $\bar{\kappa}$ for all samples, with renormalized $g_1(\bar{\beta})$'s.]

3. *Limits on deviations from a Z^2 dependence*

Figures 9 and 11–14 show the radiator sample data after all subtractions and geometrical corrections. Regression analysis of these (linear) curves determined the refractive indices n_0^* and radiator efficiencies κ^* that gave the best straight line fits, along with the one standard deviation parameter errors Δn_0 and $\Delta\kappa$. All data point errors are comparable to the dot size in the figures. Results for the independent samples

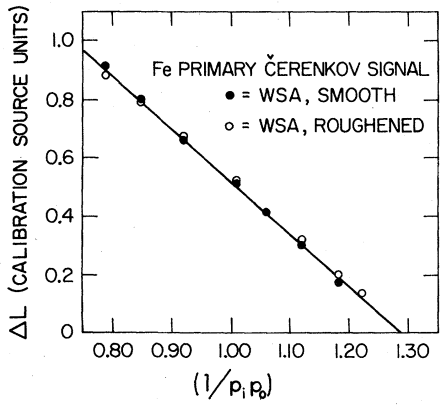

FIG. 11. Primary Čerenkov light outputs vs $(1/p_i p_0)$ for both smooth and roughened WSA samples exposed to Fe. These two data sets are used to generate a $(1/p_i p_0)$-dependent, Z-independent ratio that will "correct" other roughened WSA data to linear form.

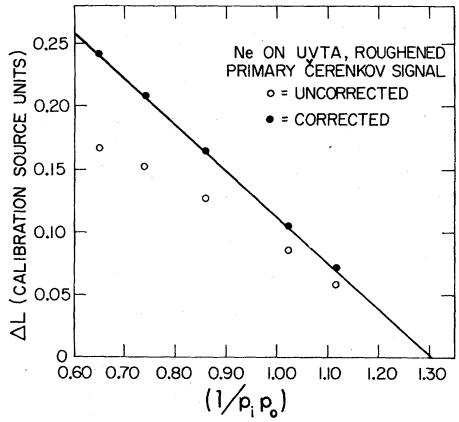

FIG. 12. Corrected (boosted) and uncorrected primary Čerenkov light output vs $(1/p_i p_0)$ for UVTA, R:Ne. No smooth sample data was taken for Ne on UVTA, necessitating this boost to linear form using the ratios of Fig. 9. An excellent fit to a line results.

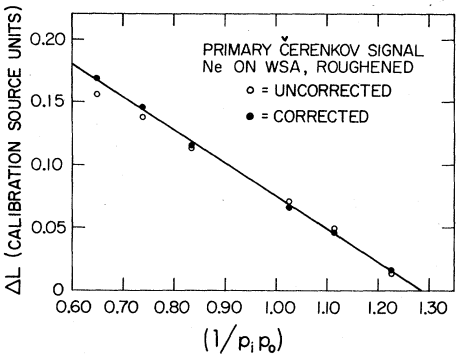

FIG. 13. Corrected and uncorrected primary Čerenkov light output vs $(1/p_i p_0)$ for WSA, R:Ne. The boost ratios of Fig. 11 are applied to these data, again providing an excellent fit to a line.

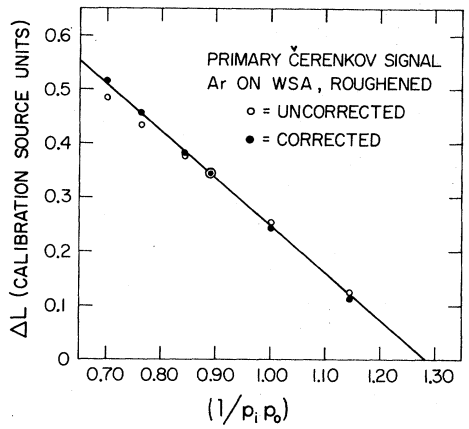

FIG. 14. Corrected and uncorrected primary Čerenkov light output vs $(1/p_i p_0)$ for WSA, R:Ar. The boost ratios of Fig. 11 are applied to the uncorrected data.

are listed in Table II. (Recall that not all samples are independent; for example, WSA, S:Fe and WSA, R:Fe are not independent, since the ratios of their data points were used to construct $g_1(\bar{\beta})_{\text{roughened WSA}}$, which was in turn used to "correct" all the WSA, R Čerenkov curves so they would form straight lines amenable to linear regression analysis.) The results are also plotted in Fig. 15. The WSA and UVTA radiator efficiencies are plotted separately; combining the two sets introduces radiator efficiency normalization errors that vitiate the increased statistical information that one set of five points normally has over partitioned sets of two and three points each.

A χ^2 analysis applied to the hypothesis of pure Z^2 dependence gives $\chi^2(\text{UVTA, R}) = 0.28$ for $\nu = 1$ degree of freedom giving $Q = 0.60$ [where $Q(\chi^2, \nu)$ is the probability integral of the χ^2 distribution], while $\chi^2(\text{WSA, R}) = 1.67$ for $\nu = 2$, giving $Q = 0.43$. Thus the data, which are of better than ~1% accuracy, are completely consistent with a pure Z^2 Čerenkov radiation output.

To place limits on the magnitude of a higher-order Z^4 term, the hypothesis $\Delta L/Z^2 \propto \kappa = \eta(1 + kZ^m)$, $m = 2$, was tested using the WSA, R data of Fig. 15. A maximum value of k was determined by rejecting the hypothesis at the 5% significance level, that is, for $\chi^2(\nu = 2) = 5.99$, resulting in $k_{\max} = 4.00 \times 10^{-5}$, $\eta = 4.28 \times 10^{-3}$. (In this treatment k is not a free parameter; hence $\nu = 2$.) The curve is displayed in Fig. 15. For Fe, $kZ^2 = 0.027$ (a 2.7% correction to ΔL relative to $Z = 1$), while for $\vec{U}$, $kZ^2 = 0.34$. Similarly, limits may be placed on the magnitude of a Z^3 term, for which $m = 1$. At the 5% significance level, we obtain $k_{\max} = 1.65 \times 10^{-3}$, $\eta = 4.22 \times 10^{-3}$.

IV. THEORETICAL ASPECTS OF HIGHER-ORDER CORRECTIONS

Frank and Tamm's classical calculation of the Čerenkov formula is based on Maxwell's equations, where the electric displacement $\vec{D}$, defined by $\vec{\nabla} \cdot \vec{D} = 4\pi\rho$, has its Fourier transform $\vec{D}(\omega)$ related to the electric field's transform $\vec{E}(\omega)$ by $\vec{D}(\omega) = \epsilon(\omega)\vec{E}(\omega)$, where $\epsilon(\omega)$ is the frequency-dependent dielectric constant. The derived field equation of interest is

$$\nabla^2\vec{A}(\omega) - (\omega^2/c^2)\epsilon(\omega)\vec{A}(\omega) = -(4\pi/c)\vec{j}(\omega), \qquad (8)$$

where $\vec{A}$ is the vector potential in the Lorentz gauge, and $\vec{j}$ is the source current corresponding to a constant velocity particle of charge Ze. Solution of this equation reveals two regimes, $\beta^2\epsilon(\omega) \lesssim 1$: for $\beta^2\epsilon(\omega) > 1$, radiation energy propa-

TABLE II. Radiator parameters determined by linear regression analysis.

Sample	$n_0^* \pm \Delta n_0$	$\kappa^* \pm \Delta\kappa$ (10^{-3})	ν, χ^2
UVTA, R: Fe (corrected)	1.5178±0.0008	(5.99±0.04)	5, 5.18
UVTA, R: Ne (corrected)	1.5187±0.0007	(5.96±0.04)	4, 6.05
WSA, R: Fe (corrected)	1.5123±0.0009	(4.34±0.03)	4, 6.27
WSA, R: Ar (corrected)	1.5111±0.0010	(4.38±0.03)	5, 2.56
WSA, R: Ne (corrected)	1.5117±0.0009	(4.32±0.04)	5, 4.34

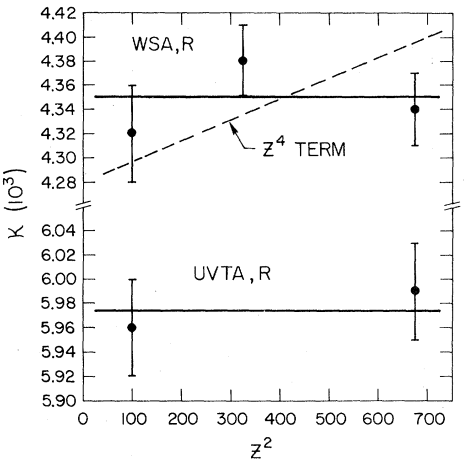

FIG. 15. Radiator efficiencies κ as a function of Z^2. The horizontal lines give a best fit to the pure Z^2 hypothesis. Assuming a Z^4 contribution, a maximum Z^4 dependence of κ (5% significance level) is shown.

gates to infinity, giving the Čerenkov phenomenon. Since $\epsilon(\omega)$ at a given frequency is assumed constant, $\vec{A}(\omega)$ is constrained to be proportional to Z, hence the Čerenkov emission, being bilinear in $\vec{A}$, is strictly proportional to Z^2.

An obvious point of attack in Eq. (8) is the assumption of a constant dielectric constant. A very crude treatment suggests that, rather than $\vec{D}=\epsilon\vec{E}$, $\vec{D}=\vec{\epsilon}\circ\vec{E}$ should be used in deriving an alternate to Eq. (8), $\vec{\epsilon}$ being a nonlinear tensorial function of $\vec{E}$. $\vec{\epsilon}$ may be estimated by considering the first few terms of the multipole expansion for the divergence of $\vec{E}$,[29]

$$\vec{\nabla}\cdot\vec{E}=4\pi\rho-4\pi\vec{\nabla}\cdot\vec{P}+4\pi\vec{\nabla}\vec{\nabla}:\vec{Q}-\cdots, \tag{9}$$

where ρ is the free charge density, $\vec{P}$ is the dipole density, and $\vec{Q}$ is the quadrupole density of the medium. For a nonpolar medium in the static limit, a single molecule's contribution to $\vec{P}$ and $\vec{Q}$ is $\vec{p}(\vec{r}_m)$ and $\vec{q}(\vec{r}_m)$, $\vec{r}_m$ being the molecular center, and $\vec{p}(\vec{r}_m)=\sum_i e_i\vec{x}_i$, $\vec{q}(\vec{r}_m)=\frac{1}{2}\sum_i e_i\vec{x}_i\vec{x}_i$, where $\vec{x}_i\equiv\vec{r}_i-\vec{r}_m$, the displacement of the ith charge element e_i from the molecular center under the action of a microscopic field $\vec{E}_{\text{micro}}$ (as opposed to the macroscopic field $\vec{E}$).[29] For a uniform field, $\vec{x}_i=\zeta_i\vec{E}_{\text{micro}}(\vec{r}_m)$, with ζ_i dependent upon molecular parameters; however, a strong field may have significant gradients, giving

$$\vec{x}_i=\zeta_i\vec{E}_{\text{micro}}(\vec{r}_m+\vec{x}_i)$$
$$\approx\zeta_i\vec{E}_{\text{micro}}(\vec{r}_m)+\zeta_i^2\vec{E}_{\text{micro}}(\vec{r}_m)\cdot\vec{\nabla}\vec{E}_{\text{micro}}(r_m).$$

By assuming that the microscopic and macroscopic electric fields are related by a constant (this is equivalent to ignoring gradients in the dielectric constant, an inconsistent but enormously simplifying assumption) we may then expect the macroscopic densities $\vec{P}$ and $\vec{Q}$ to have roughly the forms

$$\vec{P}(\vec{r})\approx\mathrm{Ne}[\zeta'\vec{E}(\vec{r})+\zeta'^2\vec{E}(\vec{r})\cdot\vec{\nabla}\vec{E}(\vec{r})]$$

and

$$\vec{Q}(\vec{r})=\tfrac{1}{2}\mathrm{Ne}\zeta'^2\vec{E}(\vec{r})\vec{E}(\vec{r})$$

to second order in ζ', a small coupling parameter. We then find from the definition of $\vec{D}$ that

$$\vec{\epsilon}(\vec{r})\approx[1+4\pi\mathrm{Ne}\zeta'-2\pi\mathrm{Ne}\zeta'^2\vec{\nabla}\cdot\vec{E}(\vec{r})]\vec{I}$$
$$+2\pi\mathrm{Ne}\zeta'^2\vec{\nabla}\vec{E}(\vec{r}),$$

where $\vec{I}$ is the unit tensor, and the operation $\vec{\epsilon}\cdot\vec{E}\equiv\vec{E}\cdot\vec{\epsilon}$. Terms proportional to Z (to second order in ζ') are thus introduced into ϵ; its effect is to introduce a perturbative current source proportional to Z^2 in Eq. (8), which in turn introduces a Z^2 component to the solution for $\vec{A}$. Any bilinear expression in $\vec{A}$ will therefore have components of order Z^3 and Z^4; if these components in the electromagnetic field energy expression remain finite at infinity, they will contribute to the Čerenkov emission intensity. Since $\zeta'\sim10^{-16}$ cm^3/esu, however, this simple classical picture suggests that any contributing higher-order terms in Z should be unmeasurably small. This is seen by calculating the maximum magnitude of $\hat{E}\cdot(\zeta'\vec{\nabla}\vec{E})$ (where $\hat{E}=\vec{E}/|\vec{E}|$), which occurs at the shock wave front of the Čerenkov cone. The radiation zone electric fields (in circular cylindrical coordinates ρ, z, ϕ) are given by (see Jelley[3])

$$E_\rho=-\frac{Ze}{c^{3/2}}\left(\frac{2}{\pi\rho}\right)^{1/2}\int\frac{(\beta^2n^2-1)^{1/4}}{\beta^{3/2}n^2}\omega^{1/2}\cos\chi\,d\omega,$$

$$E_z=+\frac{Ze}{c^{3/2}}\left(\frac{2}{\pi\rho}\right)^{1/2}\int\frac{(\beta^2n^2-1)^{3/4}}{\beta^{3/2}n^2}\omega^{1/2}\cos\chi\,d\omega,$$

and

$$E_\phi=0,$$

where

$$\chi=\omega\left(t-\frac{(z\cos\theta+\rho\sin\theta)}{c/n}\right)+\pi/4,\quad\cos\theta\equiv1/\beta n.$$

For simplicity, $n(\omega)=n_0$ is assumed, and the frequency integral is cut off at $\omega=\omega_c$, i.e., the higher-frequency components are assumed to be absorbed by the medium and therefore do not contribute to the field strength at distances (from the projectile) large compared to the $\omega>\omega_c$ absorption length of the medium. Neglecting factors of order unity, one obtains

$$\zeta'|\hat{E}\cdot\vec{\nabla}\vec{E}|\sim\frac{\omega_c^{3/2}}{\rho^{3/2}}\frac{Ze}{c^{3/2}}\zeta'.$$

Taking $\rho \sim c/\omega_c$, one gets a Z^3 contribution of $\sim 10^{-10}\, Z$.

Although this rough classical picture indicates the absence of any detectable higher-order contributions to the Čerenkov intensity, one may question whether there exist quantum mechanical corrections of any significance. One way of tackling this problem is to try to extend the rules of quantum electrodynamics so they are valid in material media as well as vacuum. Many authors have attempted this (e.g., Refs. 4–6; see Ref. 5 for additional references therein); for example, Brevik and Lautrup[5] derive a covariant field Lagrangian that yields Maxwell's equations for a nondispersive dielectric medium. Using the canonical field quantization procedure, a QED of material media is developed. The vacuum-forbidden emission of a photon by a Dirac particle becomes allowed when their modified photon propagator and external photon factor are used; the transition rate directly gives the classical Čerenkov formula in a first-order calculation. Application of the theory to higher order may present difficulties, however, due to the gross phenomenological basis of the theory. How is one to interpret the standard vacuum polarization, projectile self-energy, and vertex corrections? Is there a renormalization scheme valid to all higher orders as is the case in vacuum? In particular, does the phenomenological parameter ϵ survive these renormalizations? There is, as well, the pragmatic difficulty in evaluating higher-order phase space integrals severely complicated by the introduction of $(\epsilon - 1) \neq 0$ elements.

Nevertheless, one can conclude from simple arguments that the lowest higher-order contributions to the Čerenkov intensity from quantum effects are proportional to Z^4 (i.e., no Z^3 correction exists) if the spatial dependence of the dielectric constant is ignored. In that case one may construct a field operator of the form

$$A_\mu(x) = \sum_{k\alpha} f_{k\alpha}(\omega, \epsilon(\omega))(a_{k\alpha}\xi_\mu^{(\alpha)} e^{i\vec{k}\cdot\vec{x}} + a_{k\alpha}^\dagger \xi_\mu^{(\alpha)} e^{-i\vec{k}\cdot\vec{x}}),$$

where the photon energy and momentum $\hbar\omega = i\hbar k_4$ and $\hbar\vec{k}$ are connected by the dispersion relation $\epsilon(\omega)\omega^2 - c^2|\vec{k}|^2 = 0$. $\xi_\mu^{(\alpha)}$ is the covariant photon polarization vector, $a_{k\alpha}(a_{k\alpha}^\dagger)$ is the annihilation (creation) operator for the photon state $|k\alpha\rangle$, the sum is over all photon states, and $f(\omega, \epsilon(\omega))$ is an appropriate normalization factor dependent upon $\epsilon(\omega)$. With an interaction Hamiltonian linear in A_μ and coupling constant Ze, the lowest-order diagram (whose amplitude is proportional to Z and gives the classical Čerenkov formula) connects the initial photon, projectile

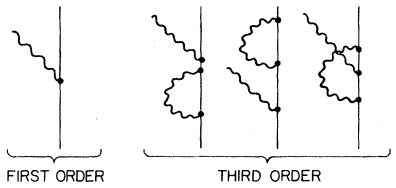

FIG. 16. The first-order diagram giving the classical Z^2 Čerenkov formula is shown, along with a few of the third-order diagrams that coherently contribute to the transition rate.

state $|0, p_i\rangle$ to the final state $|k\alpha_f, p_f\rangle$, where $(p_i - p_f - k_f) = 0$. One can deduce that the only other diagrams that add coherently to this one are of odd power in Ze, (see Fig. 16) by considering the amplitude factors

$$\langle k_f \alpha_f | \prod_{i=1}^{m} Ze \sum_{k\alpha} (a_{(i)} + a_{(i)}^\dagger) | 0 \rangle ,$$

$$m = 1,\ 2,\ 3, \ldots .$$

Thus the transition rate will consist only of even powers of Z.

To our knowledge, the only treatment of higher-order corrections to the Čerenkov intensity has been performed by Tsytovich.[7] He derives a significant Z^4 correction term by considering the effect of virtual photon emission and absorption by a Dirac particle projectile in the medium.[8] This work is quite complex, and according to Fano[30] was met by members of the National Academy of Sciences Subcommittee on Penetration of Charged Particles in Matter with "considerable difficulty in trying to understand the details of this work and to appreciate its significance." We have estimated the fractional Tsytovich correction to Čerenkov intensity at $\beta = 0.8$ and have found its magnitude to be about 2% for $Z = 1$. If it is the case, as one would be led to believe from Tsytovich's calculation, that this correction only depends on the charge of the projectile and not its mass, then this correction for iron nuclei would be 676 times larger than for electrons. Clearly, the numerous observations of cosmic ray iron nuclei with Čerenkov counters[31] preclude an effect of this magnitude. This discrepancy may be due to our treatment of a nucleus as a simple Dirac particle, or perhaps to a misinterpretation of Tsytovich's complex results.

We can only conclude that there does not seem to be at present a firm theoretical basis for either rejecting or anticipating higher-order corrections to the Čerenkov intensity of relativistic highly charged ions. Thus, examination of experimental data seems to be the only way at present to place limits on these correction terms.

V. RADIATOR SCINTILLATION

Radiator scintillation emitted along with Čerenkov radiation by a Čerenkov radiator is usually considered a contaminant light source that must be subtracted during data analysis. Therefore, a desirable feature of a radiator is that its scintillation to Čerenkov light output ratio (usually given at $\beta \sim 1$) be as small as possible. Table I lists the radiator scintillation outputs from the various radiators tested. The maximum ("peak") value corresponds to the ion stopping near the interior edge of the radiator. The plateau value is the scintillation output at ~300 MeV/amu entrance energy into the radiator (just before the onset of primary Čerenkov radiation). These values are strictly radiator scintillation; all other light sources have been subtracted. The large errors associated with these values are far larger than those associated with the radiator Čerenkov light levels; this is due to the subtraction procedure used whereby substantial error cancellation occurs for the Čerenkov light levels.

One can clearly see from the table that the presence of a wave shifter dramatically enhances the radiator scintillation levels (despite the addition of scintillation quenching agents added to inhibit wave-shifter scintillation). Also from the table one sees that the non-wave-shifted samples (UVTA) have larger Čerenkov signals than those of the wave-shifted samples (WSA). (The $\beta = 1$ Čerenkov signal values are determined by extrapolation of Figs. 6 and 7.) This is due to the use of quartz-window PMT's and to the particular experimental configuration, whereby only one side of the radiator is visible to the PMT's. This diminishes the contribution of the isotropically reradiated wave-shifted light of the WSA radiators. For maximal absolute Čerenkov light output, the choice between a wave-shifted or non-waveshifted radiator thus depends upon the PMT spectral response curve and the experimental configuration. For a minimal scintillation-to-Čerenkov light output ratio, a non-wave-shifted radiator is recommended.

From Table I we also see that the scintillation component exhibits the familiar saturation phenomenon characteristic of condensed phase (liquid and solid) scintillators in general.[11] Thus the radiator scintillation, unlike the Čerenkov light output, does not scale as Z^2, but provides a less than linear increase in light output with energy deposition. This is seen by examining the larger signals of WSA, R:Fe and WSA, R:Ar. Thus, as the projectile charge increases, the scintillation-to-Čerenkov light output ratio decreases.

VI. CONCLUSIONS

Our measurements of the Čerenkov light outputs caused by relativistic Ne, Ar, and Fe ions passing through a variety of radiators show no evidence for the existence of higher-order Z^3 or Z^4 terms in the Čerenkov emission intensity formula. The results are completely consistent (68% confidence level) with a pure Z^2 response. The upper limit placed on the Z^3 fractional coefficient, $k = 1.65 \times 10^{-3}$, although small, is still far larger than expected from our simple classical picture. Since purely quantum effects presumably cannot contribute to a Z^3 correction, we believe any Z^3 component to be so small as to be undetectable.

The upper limit placed on the Z^4 fractional coefficient, $k = 4.00 \times 10^{-5}$, has no accompanying firm theoretical limit. The only quantum calculation of a Z^4 effect is that of Tsytovich, which, if we have correctly evaluated its magnitude, predicts a fractional coefficient $k \sim 0.02$. This is far larger than our limit. It is an interesting coincidence that our experimental limit of k happens to be $\sim \alpha^2 (\alpha \equiv e^2/\hbar c)$, which is what one might naively expect of an interfering higher-order quantum effect involving two additional interaction vertices. Of course, the actual value for k may be far smaller, but at the present we can do no more than state our experimental limit, which perhaps may challenge further theoretical and experimental work to determine if a significant or detectable Z^4 contribution exists at high charge.

ACKNOWLEDGMENTS

We wish to thank Professor P. Buford Price for a critical reading of the manuscript, and for his continual support and encouragement. We also thank the staff of the Lawrence Berkeley Laboratory's Bevalac for their outstanding support, and in particular the members of the Biomedical Group for their ready cooperation in our use of their facilities. We thank Dr. Ray Hagstrom for a conversation on possible mechanisms producing a Z^3 effect. This work was supported by the Department of Energy Contract No. At(04-3)-34 and the Terradex Corporation.

[1]I. M. Frank and I. E. Tamm, Dok. Akad. Nauk SSSR 14, 109 (1937).
[2]E. Fermi, Phys. Rev. 57, 485 (1940).
[3]J. V. Jelley, *Čerenkov Radiation and Its Applications* (Pergamon, New York, 1958).
[4]J. M. Jauch and K. M. Watson, Phys. Rev. 74, 950 (1948).
[5]I. Brevik and B. Lautrup, Kgl. Danske Videnskab. Selskab Mat. Fys. Medd. 38, 1 (1970).
[6]J. Schwinger, W-Y. Tsai, and T. Erber, Ann. Phys. 96, 303 (1976).
[7]V. N. Tsytovich, Dok. Akad. Nauk. SSSR 144, 310 (1962). [Sov. Phys. Dokl. 7, 411 (1962)].
[8]V. N. Tsytovich, Zh. Eksp. Teor. Fiz. 42, 457 (1962) [Sov. Phys.—JETP 15, 320 (1962)].
[9]J. Tueller, P. L. Love, M.H. Israel, and J. Klarmann, Astrophys. J. 228, 582 (1979); P. H. Fowler, M. R. W. Masheder, R. T Moses, R. N. F. Walker, and A. Worley, Proceedings of the 16th International Cosmic Ray Conference, Kyoto, 1979 12, 338; 12, 46.
[10]Manufactured by Nuclear Enterprises, Inc., San Carlos, Calif., U. S. A.
[11]J. B. Birks, *Photophysics of Aromatic Molecules* (Wiley-Interscience, London, 1970); *The Theory and Practice of Scintillation Counting* (Pergamon, Oxford, 1964).
[12]S. P. Ahlen, B. G. Cartwright, and G. Tarlé, Nucl. Instrum. Methods 136, 229 (1976).
[13]M. J. Berger and S. M. Seltzer, NASNRC Publ. 1133, 205 (1964).
[14]E. J. Kotetich and R. Katz, Phys. Rev. 170, 391 (1968).
[15]J. B. Schutt, J. F. Arens, C. M. Shai, and E. Stromberg, Appl. Opt. 13, 2218 (1974).
[16]S. P. Ahlen, B. G. Cartweight, and G. Tarlé, Nucl. Instrum. Methods 143, 513 (1977).
[17]M. H. Salamon and G. Tarlé, Nucl. Instrum. Methods 161, 147 (1979).
[18]J. Menefee and Y. Cho, IEEE Trans. Nucl. Sci. Vol. NS-13, No. 3, 159 (1966).
[19]S. P. Ahlen, B. G. Cartwright, and G. Tarlé, Nucl. Instrum. Methods 136, 235 (1976).
[20]Nuclear Enterprises, Inc. specification sheet for Pilot 425 Čerenkov radiator.
[21]M. Cantin *et al.* in *Proceedings of the 14th International Conference on Cosmic Rays, Munich*, 1975, Münich, edited by Klaus Pinkau (Max-Planck-Institute, München, 1975), Vol. 9, p. 3205.
[22]M. H. Salamon, Lawrence Berkeley Laboratory Report No. 10446 (1980).
[23]S. P. Ahlen, Phys. Rev. A 17, 1236 (1978).
[24]G. Tarlé and M. Solarz, Phys. Rev. Lett. 41, 483 (1978).
[25]Range-energy measurements made during these runs confirm the conclusions of Ref. 24 (unpublished).
[26]J. A. Lezniak, Nucl. Instrum. Methods 136, 299 (1976).
[27]S. P. Ahlen and M. H. Salamon, Phys. Rev. A 19, 1084 (1979).
[28]I. B. Berlman, *Handbook of Fluorescence Spectra of Aromatic Molecules* (Academic, New York, 1965). The specific waveshifter used in Pilot 425 is proprietary information. The spectrum of nearly identical wave shifter, bis(isopropylstyryl)-benzene, was used.
[29]C. J. F. Böttcher, *Theory of Electric Polarization* (Elsevier, New York, 1973), Vol. 1.
[30]U. Fano, *Studies in Penetration of Charged Particles in Matter* (National Academy of Sciences—National Research Council, Washington, D. C., 1964), p. 281.
[31]G. Tarlé, S. P. Ahlen, and B. G. Cartwright, Astrophys. J. 230, 607 (1970).